MAPPING NEWLY INUNDATED AREAS IN POST-FLOOD LANDSAT IMAGES USING THRESHOLDING TECHNIQUES

Ramesh Sivanpillai[1]*, Maria Oreshkina[1], Paden Bear[2], Isaac Boettcher[3], Tyler Bradshaw[4], Isaac Coleman[5], Jessica Gifford[6]

[1]Wyoming GIS Center, ORCID: 0000-0003-3547-9464 - sivan@uwyo.edu, moreshki@uwyo.edu, [2]Rangeland Ecology & Water Management - pbear@uwyo.edu, [3]School of Energy Resources - boet.isaa177@gmail.com, [4]Department of Plant Sciences - tyler.bradshaw@att.net, [5]School of Environment and Natural Resources - isaac.d.coleman@gmail.com, [6]Department of Geology and Geophysics - jessicaegifford@gmail.com, University of Wyoming, Laramie, WY 82071. USA.

KEY WORDS: Floods, Satellite images, NDWI, MNDWI, Flood mapping.

ABSTRACT:

Identifying newly inundated areas following flood events is essential for planning rescue missions. These maps must be generated quickly as the spatial extent of the inundated areas might change during a single flood event. Several methods exist for generating such maps and several rely on one or more geospatial data to exclude existing waterbodies in an affected area. In this study, we tested a rapid flood mapping method that uses a pair of pre- and post-flood satellite images on seven sites throughout the US. We derived Normalized Difference Water Index (NDWI) and Modified NDWI (MNDWI) images from pre- and post-flood Landsat images and identified the optimal threshold values that highlighted newly inundated areas at these sites. The accuracy of the inundation maps was determined using manually interpreted verification data from the pairs of satellite images. Image analysts have identified the optimal threshold values between 25 and 40 minutes. Maps of newly inundated areas derived from differencing MNDWI and NDWI images had higher overall accuracy > 93%. Results obtained in this study confirms the utility of this rapid flood mapping technique to identify inundated areas using pre- and post-flood satellite images.

1. INTRODUCTION

Satellite images collected by active and passive sensors are used for mapping inundated areas (Goldberg et al., 2018). Multispectral images collected by passive sensors can be used when flooded areas are covered by clouds and shadows. Also, during a flooding event these maps must be updated when the extent of inundated areas changes (Sivanpillai et al. 2017). The chances of acquiring multispectral data are higher since there are relatively more passive sensors than active ones.

Several digital image processing techniques are available for identifying inundated areas in post-flood satellite images collected by optical/multispectral sensors. (Figure 1).

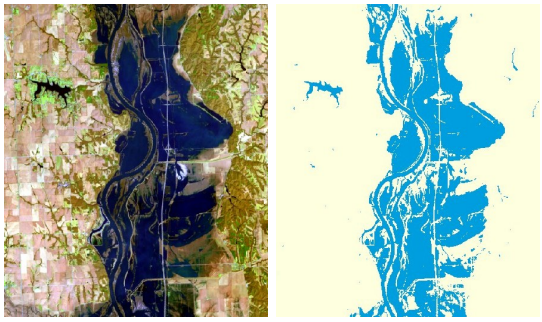

Figure 1. The post-flood satellite image (left) was used for generating the inundation map (right). One of the disadvantages of such maps is that they overestimate the flooded areas by including pre-existing waterbodies in the affected region.

Using statistical clustering or machine learning algorithms, analysts distinguish and combine pixels corresponding to water or inundated areas to generate flood maps (Amarnath, 2014; Shaw et al., 2017). Flood maps often include pre-existing water bodies in addition to highlighting newly inundated areas due to their spectral reflectance properties (Figure 2). If several waterbodies existed in an area prior to the flooding event they will be highlighted as inundated areas in these maps which will reduce their overall value for disaster response.

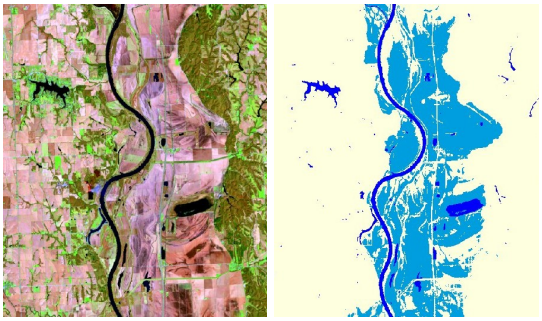

Figure 2. Existing waterbodies (left) in the impacted area are included in the inundation map (right) generated with the post-flood satellite image. Newly inundated areas are highlighted in light blue and pre-existing waterbodies are shown in dark blue.

Geospatial modelling techniques can be used for removing or recoding pre-existing waterbodies in the flood affected areas. These techniques rely on existing land cover/use (LCLU),

* Corresponding author

elevation (Wang et al., 2002; Rosser et al. 2017), or other relevant geospatial data to model pre-existing waterbodies. For example, pixels in the inundation maps that were labelled as ponds, lakes, or rivers in the LCLU map, can be reassigned to non-flooded class. However, these methods are limited to areas where current LCLU or elevation data are available. Current LCLU maps are not available for all regions or countries. Using old LCLU maps for identifying pre-existing waterbodies can lead to erroneous results. Similarly, modelling water level with digital elevation models will require more computing resources and time, which can delay the generation and delivery of inundation maps to emergency response and management agencies.

Sivanpillai et al. (2021) proposed a differencing technique to identify newly inundated areas using a pair of water indices (normalized difference water index – NDWI (McFeeters, 1996) and modified NDWI (MNDWI) (Xu, 2006). These indices were derived from multispectral images acquired before and after the flood.

$$\Delta NDWI = NDWI\ post\text{-}flood - NDWI\ pre\text{-}flood \quad (1)$$

$$\Delta MNDWI = MNDWI\ post\text{-}flood - MNDWI\ pre\text{-}flood \quad (2)$$

The NDWI (or MNDWI) values of the newly inundated areas in the post-flood image will *increase* compared to the corresponding pixel values in the pre-flood images. Hence, ΔNDWI values will be positive. On the other hand, the NDWI (or MNDWI) values of existing waterbodies and land areas may not change much in the post-flood image. For these two conditions ΔNDWI (or ΔMNDWI) will change minimally. Finally, there could be areas in the pre-flood image that were covered in water but not in the post-flood image. For these pixels, the ΔNDWI (or ΔMNDWI) values will be negative. Of these 4 outcomes, only the first one corresponds to newly inundated areas.

Identifying a threshold value for increase in NDWI (or MNDWI) value will identify newly inundated areas. Pixels that witnessed increase in NDWI (or MNDWI) above the threshold value will correspond to newly inundated areas. Thus, non-flooded areas and pre-existing waterbodies in the affected areas can be excluded. Sivanpillai et al. (2021) tested this method in five sites. However, those five sites included a limited set of flood conditions. This study expanded to include a wider range of flood conditions (urban and rural areas, clear and turbid flood waters, etc.). The primary objective of this study was to assess the effectiveness of this technique for seven new sites in the US.

2. MATERIALS AND METHOS

2.1 Pre- and Post-flood Landsat images

Eight Landsat Operational Land Imager (OLI) scenes were downloaded from the US Geological Survey's EarthExplorer website (Table 1). Pixel values in these terrain corrected images were stored as digital numbers (DNs). Path and row numbers of the scenes in Worldwide Reference System (WRS2) are listed in Table 1.

From these scenes, seven pairs of pre- and post-flood subset images were generated (Table 1). All subset images were free of clouds or shadows. When displayed in natural color infrared combination, water appeared in shades of blue color (Figure 3).

Site #	Path/Row #	Pre-flood	Post-flood
1	22/34	2016/03/29	2018/03/03
2	27/32	2018/04/23	2019/04/26
3	22/34	2016/03/29	2018/03/03
4	22/38	2016/02/26	2020/02/21
5	22/38	2016/02/26	2020/02/21
6	28/32	2017/04/11	2019/04/01
7	28/32	2017/04/11	2019/04/01

Table 1. Path and row numbers and acquisition dates of the pre- and post-flood Landsat 8 subset images used in this study.

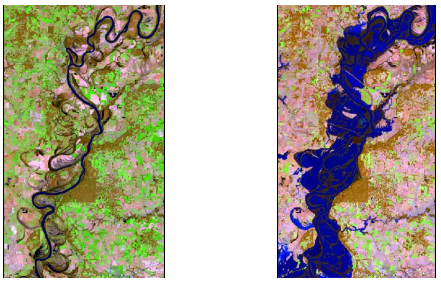

Figure 3. Pre- and post-flood subset images displayed in natural color infrared combination for study site #1 acquired by Landsat 8 OLI on 2016/03/29 and 2018/03/03 respectively.

2.2 Images of Water Indices

NDWI and MNDWI images were derived from seven pairs of Landsat subset images. For Landsat OLI images, spectral bands 3 (green) and 5 (near infrared) were used computing NDWI, while MNDWI values were computed using bands 3 (green) and 6 (shortwave infrared1).

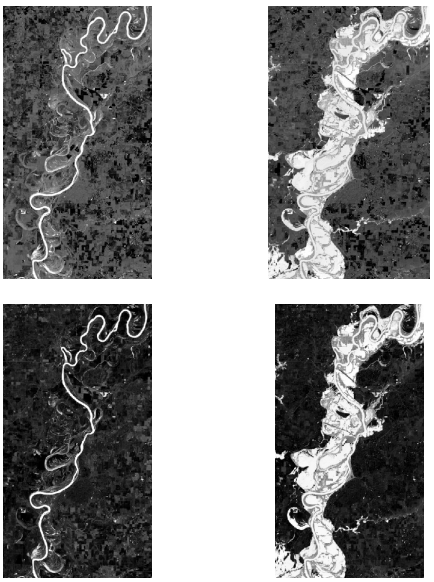

Figure 4. NDWI (top row) and MNDWI (bottom row) images derived from the pre- and post-flood Landsat 8 images for study site #1. The value of both water indices increased for the inundated areas in the post-flood image and appears in lighter shades of grey.

Since both water indices are normalized, the pixel values ranged between -1 and +1. In these images, pixel values below 0 corresponded to non-water while those above 0 were associated with water bodies (Figure 4).

2.3 Optimal Threshold Value

Optimal threshold value that highlighted newly inundated areas was identified through an iterative process. In the first iteration, a 50% value was set as the threshold value for identifying pixels with corresponding increase in values between pre- and post-flood NDWI images for a study site (Figure 5). The output image was visually compared to the pair of multispectral images for that site.

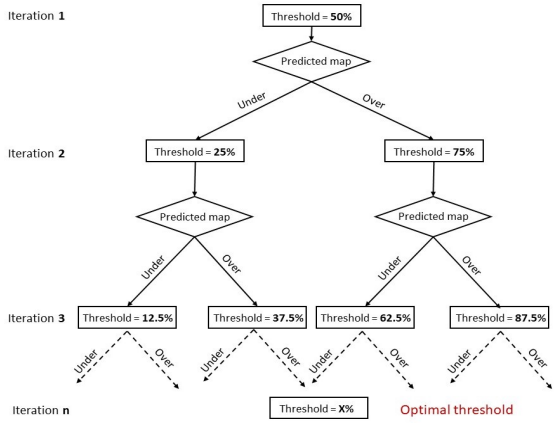

Figure 5. Iterative steps used for identifying the optimal threshold values that highlighted the newly inundated areas in a pair of pre- and post-flood NDWI (and MNDWI) images.

If the inundated areas identified in the output were less when compared to the post-flood multispectral image, then the threshold value was lowered to 25% (mid-point between 0% and 50%) for the second iteration. Lowering the threshold value would allow more pixels to meet the criteria or to be identified as inundated areas. On the other hand, if the inundated areas identified in the output were more than the actual extent observed in the post-flood image, the threshold value was increased to 75% (mid-point between 50% and 100%) for the next iteration. A higher threshold value would decrease the number of pixels that would be identified as inundated areas.

Output image generated from the 25% (or 75%) threshold value was visually compared to the pair of multispectral images. If the output image from the second iteration underpredicted the inundated areas, the threshold value was lowered to 12.5% (or 62.5%). On the other hand, if the output image from second iteration overpredicted the inundated areas, the threshold values were increased to 37.5% (or 87.5%). After evaluating the output from the 3rd iteration, threshold values were either lowered or increased as necessary (iteration 3). This process was repeated until the optimal threshold value for each NDWI image pair was identified. The optimal threshold value for each MNDWI image pair was identified using identical steps.

2.4 Accuracy Assessment

An image analyst who was not associated with identifying the optimal threshold values visually interpreted the pre- and post-flood Landsat images. It is recommended to collect verification data either from the ground or higher spatial resolution images. However, collecting field data in a timely fashion during the flood event is not feasible. Also, the chances of simultaneously acquiring high and medium spatial resolution images for a given area during floods is very rare. Temporal differences in acquisition dates can also lead to different spatial extents of inundated areas. As more imagery collected by platforms such as Planet® becomes available, it would be possible to collect verification data from high spatial resolution images for assessing the accuracy of the maps generated from moderate spatial resolution data.

This study generated reference data as randomly created points on the pre- and post-flood Landsat images in 7 sites. To create the reference points for the 7 sites, area calculations for each site were made separately. The reference points were created based on the percentage taken from the area. All the generated points were randomly distributed on the image and were separated by 500 meters from each other. In some cases, randomly distributed points were patched in one area; those points were manually moved to the more open spaces to have approximately equal distribution. All multispectral images pre- and post-flood were viewed in a different spectral resolution using various bands combinations. The reference data (points) were created through the ArcGIS Pro software.

Each point can be labelled as a) Land in both pre- and post-flood images, b) Water in both pre- and post-flood images, c) Land in pre- and Water in post-flood image, or d) Water in pre- and Land in post-flood image. Among these four combinations, points from the third combination (Land in pre-flood and Water in post-flood) were categorized as *flood* points. Rest of them were categorized as *non-flood* points (Table 2).

Site Number	Flood Points	Non-flood Points	Total Points
1	69	161	230
2	69	156	225
3	86	128	214
4	26	204	230
5	48	200	248
6	81	195	276
7	53	190	243

Table 2. Verification data points interpreted by an independent analyst using the pre- and post-flood Landsat 8 images for the seven study sites.

Error or confusion matrices were generated by comparing the verification data for each site with the inundation maps generated using changes in ΔNDWI and ΔMNDWI values. From each confusion matrix, overall, producer, and user accuracy metrics were computed to assess the performance of this technique to identify newly inundated areas (Story and Congalton, 1986).

3. RESULTS AND DISCUSSION

The Image differencing technique with optimal threshold value for each pair of NDWI (and MNDWI) images was able to highlight newly inundated areas. Five different analysts, working independently, identified the optimal threshold values for each site and pairs of images.

Image analysts determined each optimal threshold value between 4 and 6 iterations, and it took them between 25 and 40 minutes to generate each flood map (Table 3).

Site Number	ΔNDWI derived maps	ΔMNDWI derived maps
1	36	40
2	30	29
3	27	29
4	32	45
5	30	37
6	28	43
7	27	22

Table 3. Optimal threshold values identified by analysts for identifying newly inundated areas based on ΔNDWI and ΔMNDWI values.

Maps that highlight newly inundated areas in the seven sites are presented in Figure 6.

3.1 Accuracy Metrics

The overall accuracy (OA) values (Table 4) of the maps derived from ΔNDWI and ΔMNDWI images were > 95%, except for two maps derived from ΔNDWI images (sites 1 and 6). The producer accuracy values for flood class ranged between 81% and 97% for ΔNDWI derived maps while the corresponding values ranged between 77% and 100% for the maps derived using ΔMNDWI values. The user accuracy values for the flood class ranged between 91% and 100% for ΔNDWI derived maps (Table 4), while the corresponding values ranged between 91% and 98% for the maps derived using ΔMNDWI values.

Site Number	ΔNDWI derived maps			ΔMNDWI derived maps		
	OA	PA	UA	OA	PA	UA
1	93.5	84	94	95.2	90	94
2	97.3	96	96	96.9	100	92
3	97.2	97	97	96.7	95	97
4	97.0	81	91	96.5	77	91
5	98.0	90	100	98.0	92	98
6	94.6	88	93	97.5	96	98
7	95.1	85	92	97.9	98	93

Table 4. Overall (OA), producer (PA), and user (UA) accuracy values of the inundation maps derived from ΔNDWI and ΔMNDWI images. The PA and UA accuracy values for flood class are reported.

The difference in the OA values for the maps derived from two water indices were not consistent for all seven sites. For four sites, ΔNDWI derived maps had marginally higher OA values than the corresponding values associated with the ΔMNDWI derived maps (Table 4).

Minor changes in the error matrix resulted in variations between OA, PA, and UA values. For example, in site #4, five flood points were misclassified as non-flood in ΔNDWI derived inundation map (PA value of 81%). In the ΔMNDWI derived inundation map six flood points were misclassified that lowered the PA value to 77%. Site #4 had the smallest increase in flood water (Figure 6), and therefore had fewer (n = 26) verification points for that class (Table 2). Hence the minor shift in the elements of the error matrix resulted in three to four percent shift in the PA values. Similarly, in site #3 one additional point (out of 86) was misclassified as non-flood in the ΔMNDWI derived map. This resulted in the PA value to drop from 96.5% in the ΔNDWI map to 93.4% in the ΔMNDWI map.

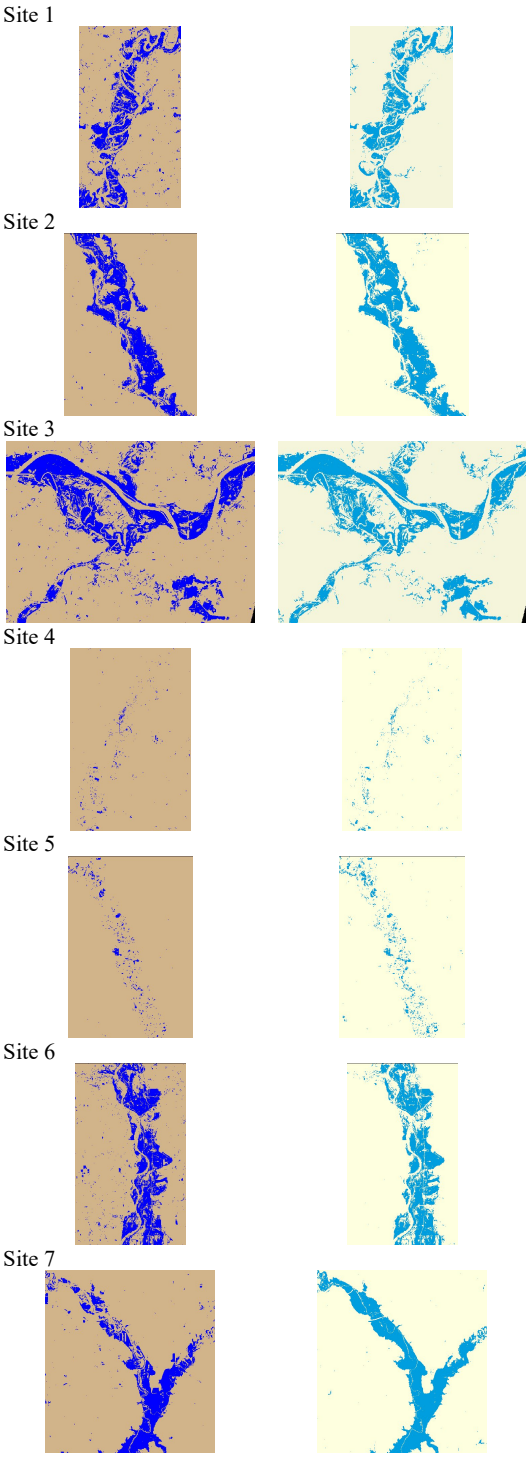

Figure 6. Maps of newly inundated areas for the seven study sites derived by differencing pre- and post-flood ΔNDWI (left) and ΔMNDWI (right) Landsat 8 OLI images.

There were relatively more non-flood verification points for all sites (Table 2). Hence minor changes in misclassification i.e., few points, did not cause major increase or decrease in the PA or UA values for the non-flood class.

Maps derived from ΔNDWI values identified several small clusters of newly inundated areas but were not present in the one derived from ΔMNDWI values. This created an impression that more areas were inundated within each site. However, during emergency response operations, managers might not focus on small, isolated clusters shown as inundated areas.

Selecting pre-flood image seasonally close to the acquisition time of the post-flood image reduced the misclassification errors. In the initial study, difference in image acquisition dates for one of the study sites (Colorado) resulted in misclassification of harvested crop fields as flooded areas (Sivanpillai et al. 2021). In this study, the pre- and post-flood images were within few days, but different years, of each other. This minimized the chances of misclassification due to differences in land use classes.

4. CONCLUSIONS

Results show that optimal threshold values obtained from differencing the pre- and post-flood water indices can identify newly inundated areas.

Maps derived from ΔMNDWI values can be used for mapping inundation maps. If data are obtained from sensors that do not acquire SWIR values, then ΔNDWI values can be used for mapping newly inundated areas.

Lower producer accuracy values for flood class obtained for inundation maps derived from both indices when the extent of flooding was small. Further research is needed to improve the accuracy of the inundation maps under low flood conditions.

Using temporally close pre-flood images is essential for minimizing the misclassification errors caused by changes in land use classes.

ACKNOWLEDGEMENTS

We thank the US Geological Survey (USGS) for providing no-cost Landsat data and supporting this work under Grant/Cooperative Agreement No. G18AP00077 to the first (RS) and second (MO) authors. Additional financial support was provided to RS, PB, IB, TB, IC, and GF by Wyoming NASA Space Grant Consortium, NASA Grant #80NSSC20M0113.

REFERENCES

Amarnath, G., 2014: An algorithm for rapid flood inundation mapping from optical data using a reflectance differencing technique. *Journal of Flood Risk Management* 7(3): 239-250.

Goldberg, M.D., Li, S., Goodman, S., Lindsey, D., Sjoberg, B, Sun, D., 2018. Contributions of operational satellites in monitoring the catastrophic floodwaters due to Hurricane Harvey. *Remote Sensing* 10(8): 1256.

McFeeters, S.K., 1996: The use of the Normalized Difference Water Index (NDWI) in the delineation of open water features. *International Journal of Remote Sensing* 17(7): 1425-1432.

Rosser, J.F., Leibovici, D.G., Jackson, M.J., 2017: Rapid flood inundation mapping using social media, remote sensing and topographic data. *Natural Hazards* 87(1): 103-120.

Shaw, R., Izumi, T., Shi, P., 2016. Perspectives of science and technology in disaster risk reduction in Asia. *International Journal of Disaster Risk Science* 74(4): 329 – 342.

Sivanpillai, R., Jacobs, K.M., Mattilio, C.M., Piskorski, E.V., 2021. Rapid flood inundation mapping by differencing water indices from pre- and post-flood Landsat images. *Frontiers of Earth Sciences* 15(1): 1-11.

Sivanpillai, R., Jones, B. K., Lamb, R.M., 2017. Accessing satellite imagery for disaster response through the International Charter: lessons learned from the 2011 US Midwestern floods. *Space Policy* 42: 54-61.

Story, M., Congalton, R., 1986: Accuracy assessment: a user's perspective. *Photogrammetric Engineering & Remote Sensing* 52(3): 397-399.

Xu, H., 2006. Modification of normalised difference water index (NDWI) to enhance open water features in remotely sensed imagery. *International Journal of Remote Sensing* 27(14): 3025-3033.

Wang, Y., Colby, J.D., Mulcahy, K.A., 2002. An efficient method for mapping flood extent in a coastal floodplain using Landsat TM and DEM data. *International Journal of Remote Sensing* 23(18): 3681-3696.